Ionosilica-based anion exchangers for low-temperature thermochemical storage of energy under mild conditions of adsorbent regeneration and saturation

Hao Wu, Peter Hesemann, Philippe Trens, Gilles Silly, Fabrice Salles*, and Jerzy Zajac*

Institut Charles Gerhardt (ICGM), Université de Montpellier, CNRS, ENSCM. Place Eugène Bataillon, 34095 Montpellier Cedex 5, France,

*E-mail: fabrice.salles@umontpellier.fr, jerzy.zajac@umontpellier.fr

ABSTRACT

Three ionosilica materials have been tested for low-temperature thermochemical storage of energy under mild conditions of adsorbent regeneration and saturation. The previous synthesis procedures were adapted to prepare materials possessing an organosilica framework with silylated cationic blocs and Cl^-, HSO_4^-, SO_4^{2-} anions in various proportions as extra-framework compensating counter-ions. Transmission and Scanning Electron Microscopy, Wavelength Dispersive X-Ray Fluorescence, Energy Dispersive X-ray Spectroscopy, Thermogravimetric analysis, adsorption of gaseous nitrogen at 77 K, ^{29}Si Solid-State Nuclear Magnetic Resonance spectroscopy were employed to establish the key characteristics of the three ionosilica samples in terms of elemental composition, particle morphology and textural properties, thermal stability and regenerability, or variability of surface activity during repeated hydration-dehydration cycles. Their capacity to adsorb water vapor at cool and moderate ambient temperatures after incomplete surface drying was demonstrated by means of the scanning microscopy operating in low-vacuum mode at 275 K, or more precisely by measuring the water adsorption isotherms at 313 K and the related differential heats under static conditions. Finally, flow calorimetry operating in the moist-gas flow mode was used to measure the integral heat accompanying the adsorption of water vapor at its partial pressure of 2.8 kPa and 296 K as well as the kinetics of heat release in three drying-saturation cycles. After a drying procedure carried out under helium flow at 353 K, the thermal performance of two ionosilica samples containing both HSO_4^- and SO_4^{2-} counter-ions was sufficient enough to consider them as potential adsorbents for auxiliary space heating in homes, small businesses, or public buildings.

Keywords: ionosilicas, water vapor adsorption, thermochemical energy storage, mild adsorbent regeneration and saturation.

1. Introduction

Low-temperature thermochemical storage of energy by heat of vapor adsorption onto solids has gained increasing attention over the last decades [1, 2]. The operating principle lies in first desorbing all gaseous components from the surface of a solid adsorbent (i.e., *charging step*) due to an energy input from the environment and then releasing the energy in the form of heat upon adsorption phenomenon when the adsorbent is subsequently put into contact with a given adsorbate (i.e., *discharging step*). Water vapor is by far the most frequently considered adsorbate in this respect and the principal criteria for adsorbent selection usually include high heats of water adsorption and improved hydrothermal stability. Besides classical hydrophilic and crystalline or amorphous adsorbents proposed in the past [3], a more recent tendency is to elaborate materials capable of adsorbing much water vapor at relatively low pressures and of being regenerated under mild temperature conditions [4-8]. With the open sorption systems operating in the moist-air flow mode, the presence of various air pollutants entering into competition with water vapor and thus diminishing the energy storage density is another important parameter that needs to be considered thoroughly [9].

The transfer of technology from research to industry has been successfully accomplished by implementing the principle of energy storage by heat of water adsorption onto zeolites in daily heating of a school building in Munich [10]. In comparison with such a short-term energy storage, the technical feasibility of seasonal storage is subject to some inherent limitations. One aspect appears critical to assuring a good efficiency of the storage technology. It is due to uncontrolled loss of adsorbent activity during an interval of several months separating the successive charging and discharging steps when the adsorbent cannot be efficiently kept away from moisture [11, 12]. To remediate this technical issue, the use of solid adsorbents which do not adsorb much water at very low vapor pressures and do not require high regeneration temperatures may be envisaged.

Ionosilicas may be potentially of great interest due to their versatility and tunable surface hydrophilic character [13]. These materials are defined as periodic mesoporous organosilicas (PMOs) synthesized exclusively from ionic silylated precursors, mostly constituted of a silylated cation and a compensating non-silylated, and thus mobile anion [14]. Ionosilicas offer huge possibilities for chemical modification and derivatization, as a virtually unlimited number of cation-anion combinations can be used to access ionosilica phases displaying various chemical compositions. In this regard, ionosilicas display a chemical polyvalence similar to that of ionic liquids and, as such, they are often considered as heterogenized ionic liquids. Besides the formation of ionosilica phases with different surface chemistries, sol-gel chemistry offers a plethora of possibilities to control the textures, architectures, and morphologies of silica-based materials [15].

The main idea behind the present study was to elaborate ionosilica phases with a particular affinity towards water vapor by taking benefit of their tunable surface properties. In order to improve the heat release performance of such materials, the substitution of the extra-framework compensating monovalent chloride anions by divalent sulfate anions was targeted. Since the enthalpy of hydration of SO_4^{2-} ions in aqueous solutions was much higher than that of Cl^- [16], it was reasonable to expect a significant increase in the heat of adsorption including, among others, the thermal effects of hydration of extra-framework anions. Classical characterization methods for siliceous materials were applied to evidence the efficiency of the surface modification, as well as evaluate the thermal stability of the resulting samples and their behavior in contact with water vapor. Batch and gas-flow calorimetry was the main tool in this study to determine the amount and the rate of heat released by ionosilicas during adsorption carried out in both static and dynamic conditions. A discussion on the improvements resulting from the ion exchange was presented to validate the use of modified ionosilica samples as

potential adsorbents in the low-temperature thermochemical storage of energy under mild conditions of adsorbent regeneration and saturation.

2. Experimental

2.1. Materials and modified ionosilica samples

The various stages leading to the preparation of ionosilica samples are depicted schematically in Scheme 1. The corresponding synthesis procedures are detailed in Supplementary material.

All materials were synthesized from *tris*-trimethoxysilylated amine (precursor **1** in Scheme 1) [15, 17]. The intermediate organosilica material **A** containing tertiary amine groups was obtained via a hydrolysis polycondensation process under nucleophilic catalysis in the presence of tetrabutylammonium fluoride solution in tetrahydrofuran as catalyst and without any structuring surfactant. This material was subsequently protonated either with hydrochloric or sulfuric acid, with the aim to achieve materials **B** and **C** possessing either chloride or sulfate/hydrogen sulfate counter-ions. Another way to obtain a sulfate containing material was considered by starting from the chloride sample **B** and modifying it via anion exchange involving sodium sulfate. This led to the **D** material potentially containing also some amount of chloride counter-ions.

The ALPHAGAZ 2 grade helium and nitrogen (Air Liquide, France) as well as the 18.2 MΩ cm ultrapure water (PURELAB® Chorus 1, ELGA Veolia) were used in the gas adsorption and calorimetry experiments.

2.2. Characterization of solid samples

The elemental composition of the three ionosilica samples was determined by referring to Wavelength Dispersive X-ray Fluorescence spectroscopy (WDXRF). A PANalytical AXIOS mAX spectrometer used to date was equipped with an SST-mAX50 X-ray source specifically

adapted for the detection of light elements, as well as a sample and cell changer for the analysis of solids and loose powders. 14 scans were collected under vacuum, each scan covering a range of the expected elements, and the peak areas of the characteristic radiations were assessed. The quantitative analysis was performed using PANalytical's proven SuperQ software and standard calibration curves for the diff erent elements. Prior to each measurement, a ionosilica sample was first dried in air at 343 K for 24 h and then carefully ground into fine particles in a mortar, mixed with powdered boric acid to confer greater mechanical resistance, and compressed for 2 min at a pressure of 8 ton m^{-2} into a 12-mm-diameter, 1-mm-thick self-supporting disc. The WDXRF analysis was repeated 3 times, each run being carried out with a freshly prepared self-supporting disc. The three measured values were subsequently averaged for each element in a given material. A high resolution low-vacuum FEI Quanta 200 FEG Scanning Electron Microscope (SEM) was used to analyze the shape and size of the ionosilica particles. The particle morphology and porosity were scanned using a FEG JEOL 2200FS Transmission Electron Microscope (TEM) operating at an acceleration voltage of 200 kV.

The adsorption and desorption isotherms for gaseous N_2 were measured at 77 K by means of a micromeritics ASAP2010 sorption equipment. Each sample was previously degassed overnight at 383 K under secondary vacuum. Whenever possible, the specific surface area was calculated on the basis of the BET model by taking 0.162 nm^2 as a cross-sectional area per adsorbed nitrogen molecule. The total mesopore volume and the mean pore diameter were determined by applying the α_S-plot procedure to the adsorption isotherm [18, 19].

The thermal stability and regenerability of the three samples were tested through thermogravimetric analysis (TGA) performed under an argon flow of 50 mL min^{-1} on a NETZSCH Jupiter STA 449 apparatus. Heating of the samples from 298 to 573 K was done in an alumina crucible with a heating ramp of 5 °C per min.

The ^{29}Si Solid-State Nuclear Magnetic Resonance (NMR) spectroscopy was employed to study the silane-silanol condensation in ionosilica samples as a function of their hydration state. For this purpose, a given solid was submitted to three consecutive dehydration-hydration cycles in a vacuum desiccator. All dehydration steps were carried out at 383 K under primary vacuum for 24 h. The hydration steps were performed under humid environment (an open recipient with ultra-pure water placed inside the desiccator) at 298 K for 48 h, with the exception of the first hydration which lasted for a week. After each single step, about 500 µL of sample were collected for the NMR analysis. The ^{29}Si NMR experiments were done first with the Cross Polarization (CP) mode combined with the Magic Angle Spinning (MAS) one to enhance the signal given by the low natural abundance of ^{29}Si nuclei. A Varian VNMRS 400 spectrometer with a magnetic field strength of 9.4 T was used. A T3 double resonance MAS probe HX with a vespel stator and ceramic 7.5 mm o.d. pencil MAS rotor were used. The experiments were performed at room temperature with a spinning rate of 5 kHz. For CPMAS spectra $\pi/2$ ^{1}H pulse duration was 5 µs, the recycle delay was set to 5 s and CP contact time to 2 ms, 128 transients were acquired under ^{1}H spinal decoupling. To render the spectra analysis more quantitative, when having the width and position of every peak fixed, single pulse experiments with 2 µs $\pi/6$ pulse duration were acquired with a recycle delay of 60 s. 300 transients were accumulated under ^{1}H spinal decoupling. The isotropic chemical shift δ_{iso} was defined as $\delta_{iso} = \frac{1}{3}(\delta_{xx} + \delta_{yy} + \delta_{zz})$ with $\delta_{ii} = \sigma_{ref} - \sigma_{ii}$ and σ_{ii} (i=x, y, z) the principal components of the shielding tensor. All solid-state NMR spectra were modelled using the DMFit program [20].

2.3. Monitoring and quantification of water vapor uptake by ionosilicas

The SEM micrographs of ionosilica samples at different hydration states were taken with the aid of the same FEI Quanta 200 FEG microscope operating in environmental (low-vacuum) mode [21]. The temperature of the environmental chamber was fixed at 275 K. The use of a

Peltier cooling plate allowed the samples to be tested under in-situ exposure to water vapor at different pressures varying successively from 200 Pa to 710 Pa.

The retention affinity and capacity of ionosilicas towards water vapor were quantified by measuring the adsorption isotherms under static conditions at 313 K using a home-made sorption apparatus described previously [22]. Prior to the sorption measurements, around 100 mg of each sample were subjected to a thermal treatment at 353 K under secondary vacuum, better than 0.01 Pa (10^{-5} Torr). The amount adsorbed corresponding to a given equilibrium pressure was calculated by following the manometric/volumetric measurement principles. The sorption measurements were performed in a Setaram C80 differential and isothermal microcalorimeter, thus allowing to simultaneously determine the quantity of adsorption and the differential molar enthalpy of adsorption [23].

The heat release kinetics and capacity of the ionosilica samples were also tested under dynamic conditions of a gas flow passing through an adsorbent bed placed in the calorimetric cell of a 4 V ms Microscal flow microcalorimeter [12]. A weighted sample (about 60 mg) was degassed directly in the calorimetric cell under a helium flow of 120 ml h^{-1} at 353 K for 24 h. Then it was cooled down to room temperature overnight under a helium flow of 120 ml h^{-1}. The flow of helium was subsequently directed to an in-line mounted saturation vessel filled with ultrapure water and thermostated by a water bath in order to be continuously saturated with water vapor at 296 K. The resulting gas mixture containing water vapor at a partial pressure of 2.8 kPa was fed continuously into the calorimetric cell where water vapor was adsorbed on the solid surface. The end of the saturation stage was set by waiting until the complete return of the thermal signal to baseline. The same degassing-saturation cycles were repeated three times for each ionosilica sample, with the total heat evolved during each saturation run corresponding to the integral heat of adsorption.

3. Results and Discussion

In view of large-scale applications, the aim of the synthesis strategy as a whole was to keep the procedures for preparation of ionosilica materials as cheap and straightforward as possible. Firstly, the organosilica intermediate containing no ionic groups (i.e., material **A**) was obtained on a 100-gram scale from the *tris*-trimethoxysilylated amine precursor *via* hydrolysis-polycondensation reaction under nucleophilic catalysis. Secondly, the target ionosilicas (i.e., materials **B**, **C**, and **D**) were achieved, in sufficient quantities for the performance of sample-consuming testing and characterization methods, by a subsequent treatment with appropriate acids. Thirdly, the template-directed synthesis to prepare porous ionosilicas with substantially higher surface areas was excluded because, on the one hand, the removal of the surfactant template from the final material may cause a great deal of difficulty and, on the other, the use of surfactants may be cost prohibitive on a larger scale. Therefore, the protocols used in the present study allowed reliable preparation of large amounts of ionosilica samples, while avoiding expensive additives and time-consuming work-up procedures. In line with expected enhancement of thermal performance due to the ionic character of potential adsorbents, materials **B**, **C**, and **D** were characterized and further tested to elucidate the effect of counter-ion on the heat release upon adsorption of water vapor under mild conditions of adsorbent regeneration and saturation.

Some representative SEM micrographs reported in Supplementary material (Fig. S1) show patterns characteristic for amorphous solid samples with polydispersed irregular particles. Examples of TEM micrographs shown in Fig. 1 reveal the absence of pores in materials **B** and **D**. Only material **C** has been found to contain some mesopores (with a mean pore radius equal to 2.4 nm); its adsorption-desorption isotherms for gaseous nitrogen measured at 77 K are reported in Fig. 1. The N_2 adsorption curve is of type IV with a tiny hysteresis loop of type H2 according to the IUPAC classification, thus indicating the existence of ink-bottle pores [24].

This sample has a non-negligible specific surface area of 85 $m^2\ g^{-1}$ due to the presence of small mesopores. The S_{BET} value obtained here is much smaller than those previously reported for other ionosilica materials which usually range between 390 and 860 $m^2\ g^{-1}$ [13, 25, 26]. Nevertheless, it should be noted that the samples used in the present studies have been prepared without using any structuring agent which is usually responsible for the creation of a porous structure in silica materials. Unexpectedly, the quantity of N_2 adsorption onto materials **B** and **D** has been close to zero (Fig. S2 in Supplementary material).

To provide clear evidence of the successful functionalization with sulfate groups, the results of chemical analysis of the three ionosilica samples based on the WDXRF study are reported in Table 1.

The observed elemental ratios are different from the ones estimated based on the theoretical formulas of the samples. There may be several reasons explaining this discrepancy. In addition to some heterogeneity of the material matrix and uncertainty arising from sample preparation for the WDXRF measurement, a greater degree of uncertainty is associated with the nitrogen content compared to those of heavier elements. The experimental errors related with this last aspect have been added to Table 1. After all, the following consideration reflects only some trends. The chloride and sulfate counter-ions have been introduced to compensate the positive charge of amine moieties. The results reported in Table 1 reveal about 47% of the residual chloride anions in the D sample. Therefore, the chloride-sulfate exchange ratio for this sample should be around 53%. Nevertheless, the sulphur content in C and D samples indicates some charge overcompensating (as evidenced by the N : S ratio, in particular). The only plausible explanation for this discrepancy is that divalent sulfate anions coexist with monovalent hydrogen sulfate ones. Within the uncertainty of the nitrogen content measurements, a great excess of SO_4^{2-} counter-ions is predicted for the two samples. The presence of FT-IR absorption bands attributed to the stretching vibration of sulfate anions may

be also considered in support of this conclusion (Fig. S3 in Supplementary material). In conclusion, the hypothetical chemical formulas of the three ionosilica materials studied in the present study are as follows: $C_9H_{19}(SiO_{1.5})_3NCl$ – material **B**; $C_9H_{19}(SiO_{1.5})_3N(SO_4)_{0.24}(HSO_4)_{0.08}Cl_{0.47}$ – material **D**; $C_9H_{19}(SiO_{1.5})_3N(SO_4)_{0.41}(HSO_4)_{0.18}$ – material **C**.

Thermal stability of the ionosilica samples is an important issue in view of their potential use in thermochemical storage. Thermogravimetric analysis gives a first order estimate of this parameter. Since ammonium-type ionosilicas had been previously shown to be thermally stable only to about 493 K [26], the present TGA experiment was conducted only until 573 K. The resulting TGA curves have been reported in Supplementary material (Fig. S4). According to the trends observed there, the thermal decomposition of amine moieties begins at 483 K for material **B** and at 523 K for the two other samples. This likely means that compensating counter-ions exert some protective effect on the thermal stability of ionosilica, probably due to stronger interactions the positively charged framework has with sulfate anions, compared to the analogous interactions with monovalent chloride ones. Amongst the arguments given for this interpretation is that the majority SO_4^{2-} counter-anion present in material **D** and particularly in material **C** has a greater polarizability compared to Cl^- one [27, 28].

Most of the physically retained water seems to be removed up to 383 K. The **B** sample appears to contain more physically adsorbed water than the two others on a per gram basis. Then, the mass loss rate significantly decreases which may indicate deep surface dehydroxylation and/or dehydration of compensating anions.

When silica gels are used in adsorption chillers, the pre-adsorption treatment is carried out at 353 K [29]. In the present study, this temperature is considered as being representative of the mild conditions of adsorbent regeneration targeted in view of the energy storage uses. It

is thus interesting to compare the mass loss values obtained at these two characteristic temperatures. The appropriate results are given in Table 2.

It is worth noting that the thermal treatment of the **B** sample at 353 K under an argon flow of 50 mL min^{-1} liberates more than 70% of such water but is not sufficient to remove it totally. In the case of sample **C**, the smallest mass loss is certainly not consistent with its highest surface area. One possibility in relation with the hydration of extra-framework counter-ions is that higher temperatures would be necessary to remove water molecules from the hydration layer of SO_4^{2-} contrary to those immobilized around Cl^-. As an illustration of energetic inputs necessary to dehydrate such anions, the Gibbs energies of hydration in aqueous solution are as follows: -340 kJ mol^{-1}, Cl^-; -330 kJ mol^{-1}, HSO_4^-; and -1080 kJ mol^{-1}, SO_4^{2-} [16].

3.1. Hydrophobic-hydrophilic properties of ionosilica surface

An analysis at microscopic level of hydration and dehydration phenomena in ionosilicas was made by referring to solid-state ^{29}Si NMR study. Materials **B** and **C** were selected for this purpose, as containing only one type of counter-ions. Each material was subjected to three consecutive dehydration-hydration cycles, as described in the Experimental section. The recorded single pulse ^{29}Si NMR spectra are reported in Figures 2 and 3, together with the results of signal deconvolution resulting in T^1, T^2, and T^3 signal components associated with organosiloxane groups $R'Si(OSi)_m(OR)_{3-m}$, m = 0,1,2,3 (see also Tables S2 and S3 for more details).

The NMR spectra of dry samples obtained after the first dehydration contain, in various proportions, three principal contributions centered at about -50, -58, and -67 ppm. They may be ascribed to different types of surface functional groups: geminal silanols (T^1 sub-structural units), isolated silanols (T^2 sub-structural units), and siloxanes (T^3 sub-structural units), respectively [30]. None of the Q^n resonances associated with organosiloxane groups

$Si(OSi)_n(OR)_{4-n}$, n = 0,1,2,3,4, can be seen in the spectra which indicates that the ammonium groups remain within the bulk of the solid phase without being broken down during the synthesis. The dried sample **B** presents more T^3 sub-structural units, thereby indicating more intense formation of Si-O-Si bonds and cross-linking of silanes to produce hydrophobic siloxane groups. The dried sample **C** with somewhat greater proportions of isolated and geminal silanols thus appears to have a more hydrophilic surface.

Further hydration stage mostly causes a noticeable decrease in the peak width. Generally, the increased mobility of a nucleus results in the motional narrowing of the related NMR peak. Already, the reduced cross-linking of functionalized silicon chains at the surface leads to their greater freedom of movement. This effect is further enhanced after hydration, likely as a result of interactions between the surface functional groups and the adsorbed water molecules. It is worth noting that the peak narrowing is much more pronounced in the case of T^1 and T^2 resonances attributed to hydrophilic silanols. Weaker interaction of the hydrated chloride and sulfate counter-ions with the ionosilica framework is also expected, as testified by the reduced polarizability of anions in aqueous solutions in comparison with their gas phase values [31]. This may also contribute to the increased mobility of functionalized silicon chains at the surface.

After the first hydration stage during which the sample remains in contact with humid atmosphere during 1 week, the proportions among the T^1, T^2, and T^3 signal components in the ^{29}Si spectra recorded on material **B** hardly change upon subsequent dehydration-hydration cycles. It may thus be concluded that the surface of this ionosilica is more resistant to water vapor and is characterized by a good reversibility of hydration and dehydration phenomena. In the case of material **C**, the proportion of the T^1 signal increases upon each hydration and decreases upon each dehydration step. Similar tendency is observed for the T^2 resonance, with the only exception of the third hydration. Since these effects are accompanied by a reversed

trend in the T^3 resonance, some opening of the siloxane bridges on the surface of material **C** by a hydroxylation mechanism to form Si-OH groups may be postulated. The reversibility of siloxane-to-silanol transformation appears to diminish with increasing number of cycles and the degree of polymerization increases.

Judging on the basis of the above results, it is important to note that the degassing conditions applied here (i.e., prolonged thermal treatment at 383 K under primary vacuum for 24 h) are already capable of inducing some dehydroxylation of the ionosilica surface. On the contrary, nothing is clear in terms of the extent to which the extra-framework counter-ions (namely Cl^-, HSO_4^-, and SO_4^{2-}) may be dehydrated. As suggested before, the main reasons behind the difference in the behavior between materials **B** and **C** include (i) enhanced cross-linking of functionalized silicon chains at the surface of material **B** as containing a greater proportion of T^3 sub-structural units, (ii) greater polarizability of the majority SO_4^{2-} anion in comparison with that of Cl^-.

3.2. Adsorption properties of ionosilica samples towards water vapor under equilibrium conditions

For the purpose of comparison among the three ionosilica samples, their potential capacity for retaining water vapor at the surface was intended to be studied under conditions of adsorption equilibrium. Usually, this is done by measuring adsorption isotherms which represent the amount of water adsorbed by unit area or mass of the solid sample as a function of the relative pressure of water vapor in the equilibrium bulk phase, p/p_0 (where p_0 is the saturated vapor pressure at a given temperature). The temperature of sample degassing (i.e., 353 K) has been chosen in line with the targeted conditions of adsorbent regeneration, as specified before. Adsorption is a temperature-dependent phenomenon and the adsorption measurements are usually performed at room temperature. Since the saturated vapor pressure of water at 293 K is

only equal to 2.34 kPa [32], the adsorption curves in the present study have been determined at 313 K in order to reduce the experimental errors due to insufficient quantity of vapor in the measuring chamber. The resulting sorption isotherms for the three ionosilica materials are presented in Fig. 4.

The adsorption curves obtained are a mixture of Type II and Type IV sorption isotherms according to the IUPAC classification [33, 34], with a portion of the curve being slightly convex upward at low relative pressure, followed by a moderate water uptake at higher relative pressures. The general shape of the adsorption isotherms suggests that the adsorption mechanism mostly follows a monolayer-multilayer formation process. The rather small specific surface area of the samples may to some extent justify the low water retention per unit mass of the adsorbent (at most, 15 wt % at saturation in the case of material **B**).

The slope of the isotherms at low relative pressures gives a good indication of the interactions operating between the sorbent and the sorbate. As discussed in the paper by Ng and Mintova [35], this linear segment tends to be vertical when the interactions are strong, whereas it becomes almost horizontal in the case of weak interactions. In the present sorption systems, the steepness of the slopes over the range of low relative pressures indicates the moderate hydrophilic character of the ionosilica surface. This is certainly because the samples have been initially activated, as they were, at 353 K under secondary vacuum. From intermediate relative pressure upwards, the quantity of adsorbed water increases steadily in a linear manner up to relative pressures of about 0.6. This linear sorption process can be explained, considering that if the adsorbed amount is proportional to the pressure, the sorption occurs without any specific interaction. Therefore, the interaction strength remains essentially the same during this sorption process. Beyond $p/p_0 = 0.6$, a significant decrease in slope of the adsorption curves is observed leading potentially to an adsorption pseudo-plateau which corresponds to the saturation of the materials. The water sorption is reversible in the case of material **C**, whereas nitrogen

adsorption has led to a clear hysteresis loop (see Figure 1). Following the paper by Morishige and Nakamura [36], the occurrence of hysteresis loops depends on different parameters, which includes the nature of adsorbate and the temperature of sorption. It is therefore difficult to predict whether a hysteresis loop can be observed in different systems. In the particular case of material **D**, a small hysteresis loop can be seen in the adsorption curve, more precisely in the p/p_0 range between 0.4 and 0.7. Additionally, it is worth noting that the desorption branches meat the adsorption ones at lower relative pressures, which makes these materials particularly promising to energy storage uses as no re-activation stage would be necessary between two sorption cycles. This point will be further developed in the last section.

As derived from the slope of the sorption isotherms at zero coverage in Fig. 4, the affinity order is as follows: material **C** < material **D** < material **B**. The extent of adsorption at any equilibrium pressure follows exactly the same order and the differences between the samples with respect to the mass of the water vapor adsorbed per unit mass of the adsorbent increase along the adsorption range studied. This observation is at variance with the highest surface area (as inferred from gaseous N_2 adsorption) of sample **C**, as well as a more hydrophilic character of its surface in comparison with that of sample **B** (as argued in section 3.1 on the basis of NMR results). In an effort to explain this discrepancy, the appearance of a hysteresis loop on the sorption isotherm for material **D** in Fig. 4 can be regarded as an indication of the presence of small pores which could be accessible to water molecules but not to nitrogen species. It should be also recalled that the vacuum treatment prior to adsorption measurements has been performed at 353 K. In light of the TGA results and the conclusions drawn from the NMR studies of hydration-dehydration cycles, the samples cannot be thus considered as being completely degassed or dehydrated. In particular, the question arises as to whether the formation of siloxane groups has already begun and whether there are still water molecules present in the hydration layers surrounding the Cl^-, HSO_4^-, and SO_4^{2-} counter-ions. The analysis

of the variations in the differential heat accompanying the adsorption of water vapor under identical conditions provides a partial answer to this question.

The curves of the differential heat of water vapor adsorption, as obtained by coupling the adsorption and calorimetry measurements in the static operation mode, are shown in Fig. 5. For a better comparison between them, they have been plotted versus the normalized adsorbed mass, this parameter being defined by dividing the mass of water vapor adsorbed at a given equilibrium pressure by the mass adsorbed at saturation (as read at $p/p_0 = 0.8$ from each sorption curve in Fig. 4).

The experimental heat values are much higher than the heat of condensation of water vapor at 313 K and they decrease with increasing normalized adsorbed masse. This clearly proves that the adsorbing water molecules still can probe the heterogeneity of successively occupied adsorption sites. At the same normalized adsorbed mass, the surfaces of the three ionosilica samples are ranked in increasing affinity order with regard to their capacity of interacting with water vapor: material **B** < material **D** < material **C**. This conclusion is not in agreement with the affinities derived from the slopes of the sorption isotherms at zero coverage. It may be explained equally well by the siloxane-to-silanol conversion being more probable at the surface of material **C** and by a partial hydration of extra-framework counter-ions providing more energy in the case of sulfate anions.

In conclusion, even if the vacuum treatment at 353 K is not capable of removing all physically adsorbed water molecules from the surface as well as all water molecules constituting the hydration layers of the extra-framework counter-ions, a significant gain in energy can potentially be obtained upon adsorption of water vapor when replacing material **B** by materials **D** and **C**. This conclusion is of great importance in view of the thermochemical storage of energy envisaged in the present study. In light of the importance of choosing an activation temperature realistic for industrial uses, the comparison between the water sorption

capacity of the present ionosilica materials with those of other solid adsorbents may be instructive. According to Fig. 4, the maximum amount adsorbed at saturation varies between 100 and 150 mg g^{-1} and it is obviously lower than the experimentally measured capacities of adsorption reported for zeolites or zeolite-like materials tested under harsher degassing conditions; e.g., 230 mg g^{-1} for synthetic nano-sized zeolites as a function of NaCl concentration after a thermal treatment at 200 °C [37], 400-600 mg g^{-1} at a p/p_0 of 32% for mesoporous modified MIL-101 materials in presence of $CaCl_2$ after a complete removal of water [8], as well as 240-600 mg g^{-1} in the case a series of different MOF structures after a desorption under vacuum [38]. Nevertheless, when the activation conditions are kept mild, the sorption performance of the present ionosilicas becomes comparable to those of 13X, LTA, mordenite or AlPO/SAPO frameworks [35,39,40].

In the event that the discharging step is to be carried out at wintertime temperatures, it seems pertinent to check the ability of ionosilicas to attract water molecules from the surrounding environment at ambient temperatures close to 273 K. Since adsorption measurements cannot be performed under such conditions, dynamic visualization of samples submitted to low pressures of water vapor varying from 200 to 710 Pa (*i.e.*, from 1.5 to 5.3 Torr) has been done by making use of an environmental scanning electron microscope operating at 275 K. It should be underlined that the volume of the environmental chamber was large enough as compared to that of the solid sample. Consequently, the water uptake by the latter hardly changed the vapor pressure within the chamber.

Some selected SEM micrographs taken at different pressures of water vapor are reported in Supplementary material (Fig. S5) for two materials **B** and **C**. The main conclusion drawn from the analysis of these images is that material **C** appears much more hygroscopic than material **B**. Indeed, a condensation of water vapor around the **C** particles is clearly observed starting from a vapor pressure of 700 Pa, irrespective of the particle size. The same observations

have been done twice on the same particles and the same dynamic behavior towards water vapor is monitored each time.

3.3. Heat release performances of ionosilicas under mild conditions of adsorbent regeneration and saturation

In the context of the thermochemical energy storage, the capacity of ionosilicas to release heat, as measured by calorimetry, is by far the most important characteristics. Since the low-temperature thermochemical storage of energy by heat of water adsorption is intended to be implemented in open sorption systems operating in the moist-air flow mode, the heat release performance of the three ionosilica materials has been tested by flow microcalorimetry. In accordance with the mild conditions of adsorbent regeneration and saturation, each sample placed in the calorimetric cell was first degassed by a continuous flow of pure helium at 353 K and then saturated with water vapor at its partial pressure of 2.8 kPa in a flow of helium. The integral heats of adsorption measured in three consecutive dehydration-saturation cycles are given in the form of histogram bars in Figure 6.

A significant improvement in the thermal performance by about 42 – 56% is observed when replacing Cl^- by SO_4^{2-} counter-ions since the average integral heat of adsorption per unit mass of the adsorbent changes from 480 kJ kg^{-1} for material **B** to 680 kJ kg^{-1} and even to 750 kJ kg^{-1} for materials **D** and **C**, respectively. Note that the last value is comparable to the highest heat values obtained by adsorbing water vapor under similar regeneration and saturation conditions onto zeolites of the 13X type modified by ion exchange with cerium and magnesium cations [11, 12].

With the exception of the case of material **B**, the integral heat of adsorption takes somewhat different values upon successive cycles. This points towards some difficulty in reproducing exactly the same regeneration conditions when the sample is degassed at 353 K by

helium flowing though the calorimetric cell during 24 h. It is worth noting that non-negligible experimental errors have been evaluated by repeating the calorimetry experiments.

It may be interesting to compare the above-mentioned heats of adsorption with the theoretical values evaluated by assuming that the thermal effects are due only to the hydration of the extra-framework compensating counter-ions. Given the theoretical chemical formulas established previously and the enthalpies of anion hydration in aqueous solutions [16], the following heat estimates are obtained: 1021 kJ kg^{-1}, material **B**; 1291 kJ kg^{-1}, material **D**; 1417 kJ kg^{-1}, material **C**. Within the framework of the present assumption (i.e., only hydration of counter-ions), it is clear that the mild conditions of adsorbent regeneration applied in the present study cannot lead to a complete dehydration of the ionosilica surface. Despite this, the integral heats of adsorption measured for the low humidity level are of the same order of magnitude as those obtained with such highly hydrophilic adsorbents as zeolites.

The time scale of the heat release is another interesting aspect of the energy storage when making use of ionosilica materials. The kinetics of heat evolvement for the two samples containing sulfate counter-ions is slower than that for material **B** (see the heat release profiles in Figure S6 in Supplementary material). The discharging (heat release) period lasts for about 10 h in the case of material **B**, whereas it extends beyond this time frame in the other cases. For material **B**, the instantaneous values of the heat released upon adsorption change in an irregular manner over time and in different cycles: the heat release is the most intensive during the first 5 h and then it passes through a series of local minima and maxima. This rather compromises the use of this sample for the reversible dehydration-hydration process. Sample **D** is characterized by a more regular heat evolvement. Here, the steep initial increase to about 0.7-0.8 kJ kg^{-1} is followed by a somewhat more gradual decay which ends at about 20 h. In the case of sample **C**, a similar rise in the heat is observed in an initial time period of 2-3 h, though the instantaneous heat release does not exceed the maximum value of 0.55 kJ kg^{-1}. Afterwards, the

heat decrease is much more gradual compared to that recorded on sample **D**. In consequence, some residual heat is released even after 30 h.

In the case of cation-exchanged zeolites, a considerably steeper increase in the heat release was observed, namely, lasting for 6-8 h and getting the maximum value in the range of 2.5-3.8 kJ kg^{-1} [12]. The heat release kinetics given by the present ionosilica samples is more gradual. Therefore, milder operating temperatures for heating systems are expected to be reached during a much longer period of time.

4. Conclusion

With the long-term aim of ensuring the stability and effectiveness of charging-discharging cycles in the energy storage by heat of sorption, ionosilica-based anion exchangers were considered as potential adsorbents capable of operating effectively in the moist-gas flow mode under conditions of low humidity levels during exothermic adsorption-saturation and moderate temperatures of adsorbent regeneration. A significant increase in the thermal performance of these materials containing silylated cationic blocs in the organosilica framework was obtained by substituting the extra-framework compensating chloride anions by sulfate ones. With the regeneration temperature equal only to 353 K and the partial pressure of water vapor of only 2.8 kPa during the saturation steps, the average integral heat of adsorption per unit mass of the adsorbent was about 700 kJ kg^{-1} for two ionosilica samples containing both HSO_4^- and SO_4^{2-} counter-ions. This put the ionosilica samples among the top performing storage materials studied for this type of applications [2, 3, 7]. Furthermore, these ionosilicas provided a more regular heat release profile for a much longer period of time when compared with cation-exchanged zeolites. Therefore, they are better suited to the construction of heat storage units for auxiliary space heating in homes, small businesses, or public buildings.

Acknowledgement:

One of the authors, H. Wu, greatly acknowledges the financial support of his work by French Ministry of National Education, Higher Education and Research. The authors want to thank Dr. N. Donzel, Dr. Ph. Gaveau, Mr. E. Fernandez, Mr. J. Fullenwarth, and Miss L. Daenens of the Platform of Analysis and Characterisation (PAC), Pôle Chimie Balard, for their assistance in N_2 adsorption, NMR, WDXRF, and IR measurements. The authors also thank the Electronic and Analytical Microscopy (MEA) Platform.

CAPTIONS TO FIGURES

Scheme 1. Simplified flowsheet of the synthesis procedures used in the present study to achieve ionosilica materials of type **B**, **C**, and **D**

Figure 1. TEM micrographs for ionosilica materials **B** (panel a) and **D** (panel b), together with the gaseous N_2 adsorption-desorption isotherms at 77 K for material **C** (panel c). Textural parameters of sample **C** inferred from the analysis of the adsorption branch based on the BET and generalized α_S-plot procedures are reported within the lower panel: BET specific surface area, S_{BET}, mesopore volume, V_{mes}, and mean mesopore diameter, d_m

Figure 2. ^{29}Si single pulse NMR spectra (black lines) recorded on material **B** submitted to three consecutive dehydration-hydration cycles. The colored lines represent the results of signal processing by deconvolution while assuming the Gaussian peak shape with a linear background so as to determine the chemical shifts and relative intensities of the T^1 (green lines), T^2 (red lines), and T^3 (blue lines) signal components. For the purpose of comparison, the same intensity scale has been used for the Y-axes.

Figure 3. ^{29}Si single pulse NMR spectra (black lines) recorded on material **C** submitted to three consecutive dehydration-hydration cycles. The colored lines represent the results of signal processing by deconvolution while assuming the Gaussian peak shape with a linear background so as to determine the chemical shifts and relative intensities of the T^1 (green lines), T^2 (red lines), and T^3 (blue lines) signal components. For the purpose of comparison, the same intensity scale has been used for the Y-axes.

Figure 4. Adsorption (filled circles) and desorption (empty circles) isotherms for water vapor measured on materials **B**, **D**, and **C** at 313 K. The ionosilica samples were activated by thermal treatment at 353 K during 8 h under a secondary vacuum.

Figure 5. Variations of the differential heat of adsorption for water vapor materials **B**, **D**, and **C** as a function of the normalized adsorbed mass (see explanation in the text) at 313 K. The

dashed line represents the evaporation enthalpy (equal to the condensation heat) of water at 313 K.

Figure 6. Integral heats of adsorption for water vapor onto materials **B**, **D**, and **C** measured at 296 K under dynamic conditions during three consecutive dehydration-saturation cycles. The experimental errors are marked as vertical bars.

TABLES

Table 1. Results of elemental analysis by WDXRF made on the three ionosilica samples used in the present study; experimental errors estimated from the sample standard deviations of the element contents are also reported. Theoretical elemental ratios are given in brackets.

Material / Elemental ratio	**B**	**D**	**C**
Si : N	4.2±0.5 (3)	3.2±0.3 (3)	3.3±0.6 (3)
N : Cl	0.6±0.1 (1)	2.7±0.4 (2)	-
N : S	-	2.8±0.6 (4)	1.7±0.4 (2)
SO_4^{2-} : HSO_4^-	-	3.0±1.0	2.3±0.8

Table 2. Percentage of mass loss monitored up to two characteristic temperatures for the ionosilica samples studied. These values were calculated on the basis of thermogravimetric analysis; the corresponding TGA curves are reported in Supplementary material (Fig. S3).

Material	**B**	**D**	**C**
		Mass loss (%)	
Total up to 383 K	14	10	8
Total up to 353 K	11	8	6
Relative up to 353 K*	80	75	71

*with respect to the mass loss up to 383 K taken as the reference value for physically adsorbed water

References

[1] K.E. N'Tsoukpoe, H. Liu, N. Le Pierrès, L. Luo, A review on long-term sorption solar energy storage, Renew. Sust. Energ. Rev., 13 (2009) 2385-2396. https://doi.org/10.1016/j.rser.2009.05.008

[2] N. Yu, R.Z. Wang, L.W. Wang, Sorption thermal storage for solar energy, Prog. Energy Combust. Sci., 39 (2013) 489-514. https://doi.org/10.1016/j.pecs.2013.05.004

[3] H. Wu, F. Salles, J. Zajac, A Critical Review of Solid Materials for Low-Temperature Thermochemical Storage of Solar Energy Based on Solid-Vapour Adsorption in View of Space Heating Uses, Molecules 24 (2019) 945. https://doi.org/10.3390/molecules24050945

[4] J. Canivet, J. Bonnefoy, C. Daniel, A. Legrand, B. Coasne, D. Farrusseng, Structure–property relationships of water adsorption in metal–organic frameworks, New J. Chem., 38 (2014) 3102-3111. https://doi.org/10.1039/C4CS00078A

[5] J. Canivet, A. Fateeva, Y. Guo, B. Coasne, D. Farrusseng, Water adsorption in MOFs: fundamentals and applications, Chem. Soc. Rev., 43 (2014) 5594-5617. https://doi.org/10.1039/C4NJ00076E

[6] A. Krajnc, J. Varlec, M. Mazaj, A. Ristić, N.Z. Logar, G. Mali, Superior Performance of Microporous Aluminophosphate with LTA Topology in Solar-Energy Storage and Heat Reallocation, Adv. Energy Mater., 7 (2017) 1601815. https://doi.org/10.1002/aenm.201601815

[7] A. Permyakova, O. Skrylnyk, E. Courbon, M. Affram, S. Wang, U.-H. Lee, A.H. Valekar, F. Nouar, G. Mouchaham, T. Devic, G. De Weireld, J.-S. Chang, N. Steunou, M. Frère, C. Serre, Synthesis Optimization, Shaping, and Heat Reallocation Evaluation of the Hydrophilic Metal–Organic Framework MIL-160(Al), ChemSusChem, 10 (2017) 1419-1426. https://doi.org/10.1002/cssc.201700164

[8] W. Shi, Y. Zhu, C. Shen, J. Shi, G. Xu, X. Xiao, R. Cao, Water sorption properties of functionalized MIL-101(Cr)-X (X=-NH2, –SO3H, H, –CH3, –F) based composites as thermochemical heat storage materials, Micro. Meso. Mater., 285 (2019) 129-136. https://doi.org/10.1016/j.micromeso.2019.05.003

[9] S. Bennici, T. Polimann, M. Ondarts, E. Gonze, C. Vaulot, N. Le Pierrès, Long-term impact of air pollutants on thermochemical heat storage materials, Renew. Sust. Energ. Rev., 117 (2020) 109473. https://doi.org/10.1016/j.rser.2019.109473

[10] A. Haji Abedin, M.A. Rosen, Energy and exergy analyses of an open thermochemical energy storage system: methodology and illustrative application, The Open Renewable Energy Journal, 5 (2012) 41–48. https://doi.org/10.2174/1876387101205010041

[11] D. Alby, F. Salles, J. Fullenwarth, J. Zajac, On the use of metal cation-exchanged zeolites in sorption thermochemical storage: Some practical aspects in reference to the mechanism of water vapor adsorption, Sol. Energy Mater. Sol. Cells, 179 (2018) 223-230. https://doi.org/10.1016/j.solmat.2017.11.020

[12] H. Wu, P. Trens, B. Fraisse, F. Salles, J. Zajac, Hydration mechanism in Ce-exchanged zeolites and heat release performances upon adsorption of water vapour in support of their potential use in thermochemical storage of energy under mild conditions of adsorbent regeneration and saturation, Micro. Meso. Mater., 296 (2020) 109999. https://doi.org/10.1016/j.micromeso.2020.109999

[13] U.D. Thach, P. Trens, B. Prelot, J. Zajac, P. Hesemann, Tuning the Interfacial Properties of Mesoporous Ionosilicas: Effect of Cationic Precursor and Counter Anion, J. Phys. Chem. C, 120 (2016) 27412-27421. https://doi.org/10.1021/acs.jpcc.6b09457

[14] P. Hesemann, T.P. Nguyen, E.H. S., Precursor Mediated Synthesis of Nanostructured Silicas: From Precursor-Surfactant Ion Pairs to Structured Materials, Materials (Basel), 7 (2014) 2978-3001. https://doi.org/10.3390/ma7042978

[15] T.P. Nguyen, P. Hesemann, T.M. Linh Tran, J.J.E. Moreau, Nanostructured polysilsesquioxanes bearing amine and ammonium groups by micelle templating using anionic surfactants, J. Mater. Chem., 20 (2010) 3910-3917. https://doi.org/10.1039/b925352a

[16] Y. Marcus, A simple empirical model describing the thermodynamics of hydration of ions of widely varying charges, sizes, and shapes, Biophys. Chem., 51 (1994) 111-127. https://doi.org/10.1016/0301-4622(94)00051-4

[17] D. Sauvanier, W.S.J. Li, N. Ferlin, P. Lacroix-Desmazes, B. Prelot, P. Hesemann, Simple and Straightforward Synthesis of Porous Ionosilica for Efficient Chromate Adsorption, Isr. J. Chem., 59 (2019) 843-851. https://doi.org/10.1002/ijch.201800153

[18] S.J. Gregg, K.S.W. Sing, Adsorption, Surface Area and Porosity, 2nd ed., Academic Press, London, 1982.

[19] M.J. Meziani, J. Zajac, D.J. Jones, J. Rozière, S. Partyka, Surface Characterization of Mesoporous Silicoaluminates of the MCM-41 Type: Evaluation of Polar Surface Sites Using Flow Calorimetry, Adsorption of a Cationic Surfactant as a Function of Pore Size and Aluminum Content, Langmuir, 13 (1997) 5409-5417. https://doi.org/10.1021/la970409a

[20] D. Massiot, F. Fayon, M. Capron, I. King, S. Le Calvé, B. Alonso, J.-O. Durand, B. Bujoli, Z. Gan, G. Hoatson, Modelling one- and two-dimensional solid-state NMR spectra, Magn. Reson. Chem., 40 (2002) 70-76. https://doi.org/10.1002/mrc.984

[21] G. Montes-H, J. Duplay, L. Martinez, C. Mendoza, Swelling–shrinkage kinetics of MX80 bentonite, Appl. Clay Sci., 22 (2003) 279-293. https://doi.org/10.1016/S0169-1317(03)00120-0

[22] N. Tanchoux, P. Trens, D. Maldonado, F. Di Renzo, F. Fajula, The adsorption of hexane over MCM-41 type materials, Colloids Surf. A Physicochem. Eng. Asp., 246 (2004) 1-8. https://doi.org/10.1016/j.colsurfa.2004.06.033

[23] P. Trens, H. Belarbi, C. Shepherd, P. Gonzalez, N.A. Ramsahye, U.H. Lee, Y.-K. Seo, J.-S. Chang, Coadsorption of n-Hexane and Benzene Vapors onto the Chromium Terephthalate-Based Porous Material MIL-101(Cr) An Experimental and Computational Study, J. Phys. Chem. C, 116 (2012) 25824-25831. https://doi.org/10.1021/jp308258k

[24] K.S.W. Sing, R.T. Williams, Physisorption Hysteresis Loops and the Characterization of Nanoporous Materials, Adsorption Science & Technology, 22 (2004) 773-782. https://doi.org/10.1260/0263617053499032

[25] M. Braun, U.D. Thach, B. Prelot, P. Hesemann, D. Esposito, Pd@ionosilica as heterogeneous hydrogenation catalyst for continuous flow reductive upgrade of cinnamaldehyde, Journal of Chemical Technology & Biotechnology, 92 (2017) 2229-2235. https://doi.org/10.1002/jctb.5278

[26] U.D. Thach, P. Hesemann, G. Yang, A. Geneste, S. Le Caër, B. Prelot, Ionosilicas as efficient sorbents for anionic contaminants: Radiolytic stability and ion capacity, J Colloid Interface Sci, 482 (2016) 233-239. https://doi.org/10.1016/j.jcis.2016.07.069

[27] P. Jungwirth, J.E. Curtis, D.J. Tobias, Polarizability and aqueous solvation of the sulfate dianion, Chem. Phys. Lett., 367 (2003) 704-710. https://doi.org/10.1016/S0009-2614(02)01782-7

[28] P. Jungwirth, D.J. Tobias, Chloride Anion on Aqueous Clusters, at the Air−Water Interface, and in Liquid Water: Solvent Effects on Cl- Polarizability, J. Phys. Chem. A, 106 (2002) 379-383. https://doi.org/10.1021/jp012059d

[29] A. Sapienza, A. Velte, I. Girnik, A. Frazzica, G. Füldner, L. Schnabel, Y. Aristov, "Water - Silica Siogel" working pair for adsorption chillers: Adsorption equilibrium and dynamics, Renew. Energ., 110 (2017) 40-46. https://doi.org/10.1016/j.renene.2016.09.065

[30] A. Ciogli, P. Simone, C. Villani, F. Gasparrini, A. Laganà, D. Capitani, N. Marchetti, L. Pasti, A. Massi, A. Cavazzini, Revealing the Fine Details of Functionalized Silica Surfaces by Solid-State NMR and Adsorption Isotherm Measurements: The Case of Fluorinated Stationary Phases for Liquid Chromatography, Chem. Eur. J., 20 (2014) 8138-8148. https://doi.org/10.1002/chem.201304330

[31] J.J. Molina, S. Lectez, S. Tazi, M. Salanne, J.-F. Dufrêche, J. Roques, E. Simoni, P.A. Madden, P. Turq, Ions in solutions: Determining their polarizabilities from first-principles, J. Chem. Phys., 134 (2011) 014511. https://doi.org/10.1063/1.3518101

[32] D.R. Lide, CRC Handbook of Chemistry and Physics, Taylor & Francis, Boca Raton, 2004.

[33] M. Thommes, K. Kaneko, V. Neimark Alexander, P. Olivier James, F. Rodriguez-Reinoso, J. Rouquerol, S.W. Sing Kenneth, Physisorption of gases, with special reference to the evaluation of surface area and pore size distribution (IUPAC Technical Report), Pure Appl. Chem., 2015, pp. 1051. https://doi.org/10.1515/pac-2014-1117

[34] J. Rouquerol, D. Avnir, C.W. Fairbridge, D.H. Everett, J.M. Haynes, N. Pernicone, J.D.F. Ramsay, K.S.W. Sing, K.K. Unger, Recommendations for the characterization of porous solids (Technical Report), Pure Appl. Chem., 1994, pp. 1739. https://doi.org/10.1351/pac199466081739

[35] E.-P. Ng, S. Mintova, Nanoporous materials with enhanced hydrophilicity and high water sorption capacity, Micropor. Mesopor. Mat., 114 (2008) 1-26. https://doi.org/10.1016/j.micromeso.2007.12.022

[36] K. Morishige, Y. Nakamura, Nature of Adsorption and Desorption Branches in Cylindrical Pores, Langmuir, 20 (2004) 4503-4506. https://doi.org/10.1021/la030414g

[37] H.M. Radman, A.A. Dabbawala, I. Ismail, Y.F. Alwahedi, K. Polychronopoulou, B.V. Vaithilingam, G.P. Singaravel, S. Morin, M. Berthod, S.M. Alhassan, Influence of salt on nanozeolite-Y particles size synthesized under organic template-free condition, Micropor. Mesopor. Mat., 282 (2019) 73-81. https://doi.org/10.1016/j.micromeso.2019.03.015

[38] H. Furukawa, F. Gándara, Y.-B. Zhang, J. Jiang, W.L. Queen, M.R. Hudson, O.M. Yaghi, Water Adsorption in Porous Metal–Organic Frameworks and Related Materials, J. Am. Chem. Soc., 136 (2014) 4369-4381. https://doi.org/10.1021/ja500330a

[39] P. Sharma, J.-S. Song, M.H. Han, C.-H. Cho, GIS-NaP1 zeolite microspheres as potential water adsorption material: Influence of initial silica concentration on adsorptive and physical/topological properties, Sci. Rep., 6 (2016) 22734. https://doi.org/10.1038/srep22734

[40] G. Basina, D. AlShami, K. Polychronopoulou, V. Tzitzios, V. Balasubramanian, F. Dawaymeh, G.N. Karanikolos, Y. Al Wahedi, Hierarchical AlPO4-5 and SAPO-5 microporous molecular sieves with mesoporous connectivity for water sorption applications, Surf. Coat. Tech., 353 (2018) 378-386. https://doi.org/10.1016/j.surfcoat.2018.08.083

Scheme 1

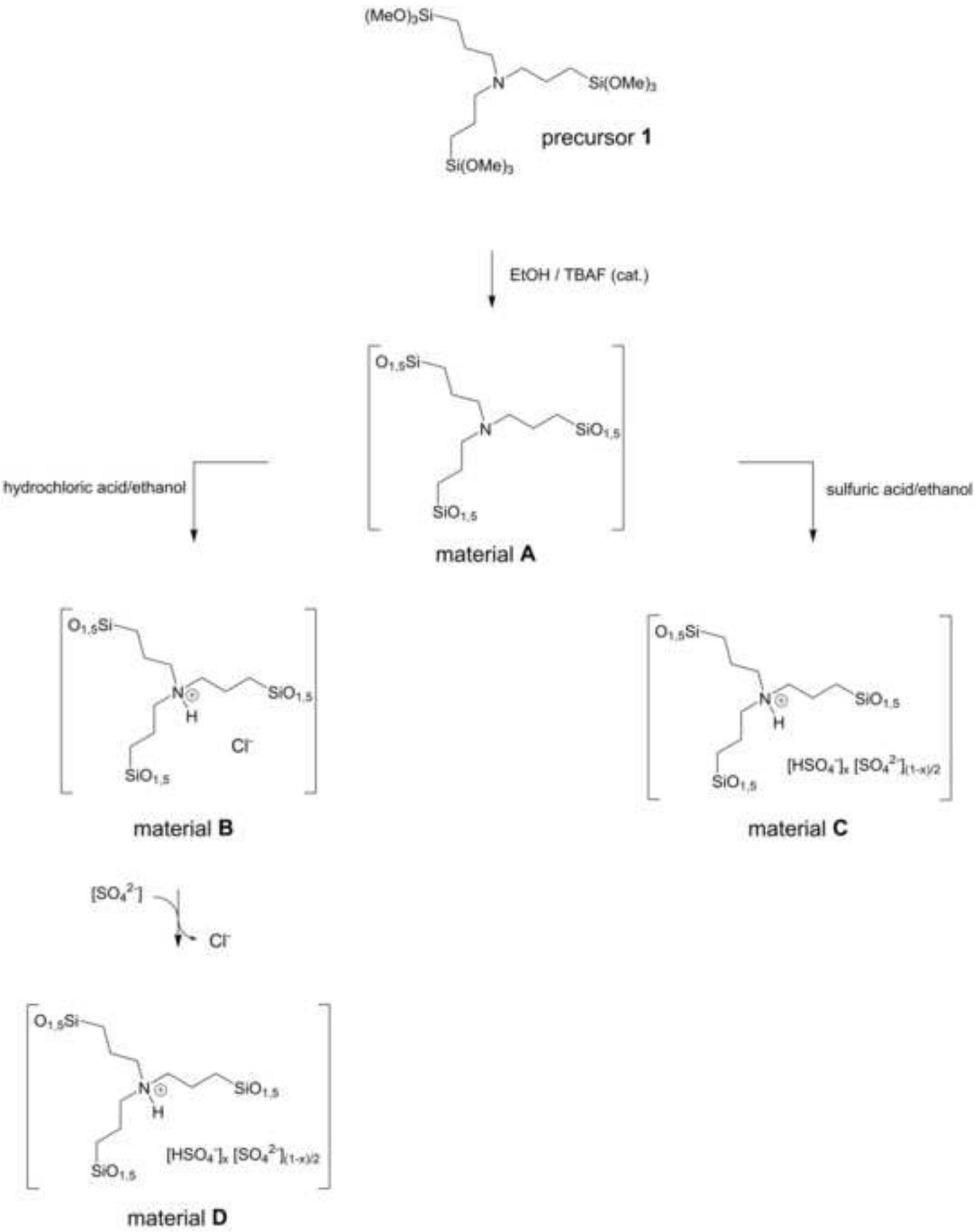

Figure 1

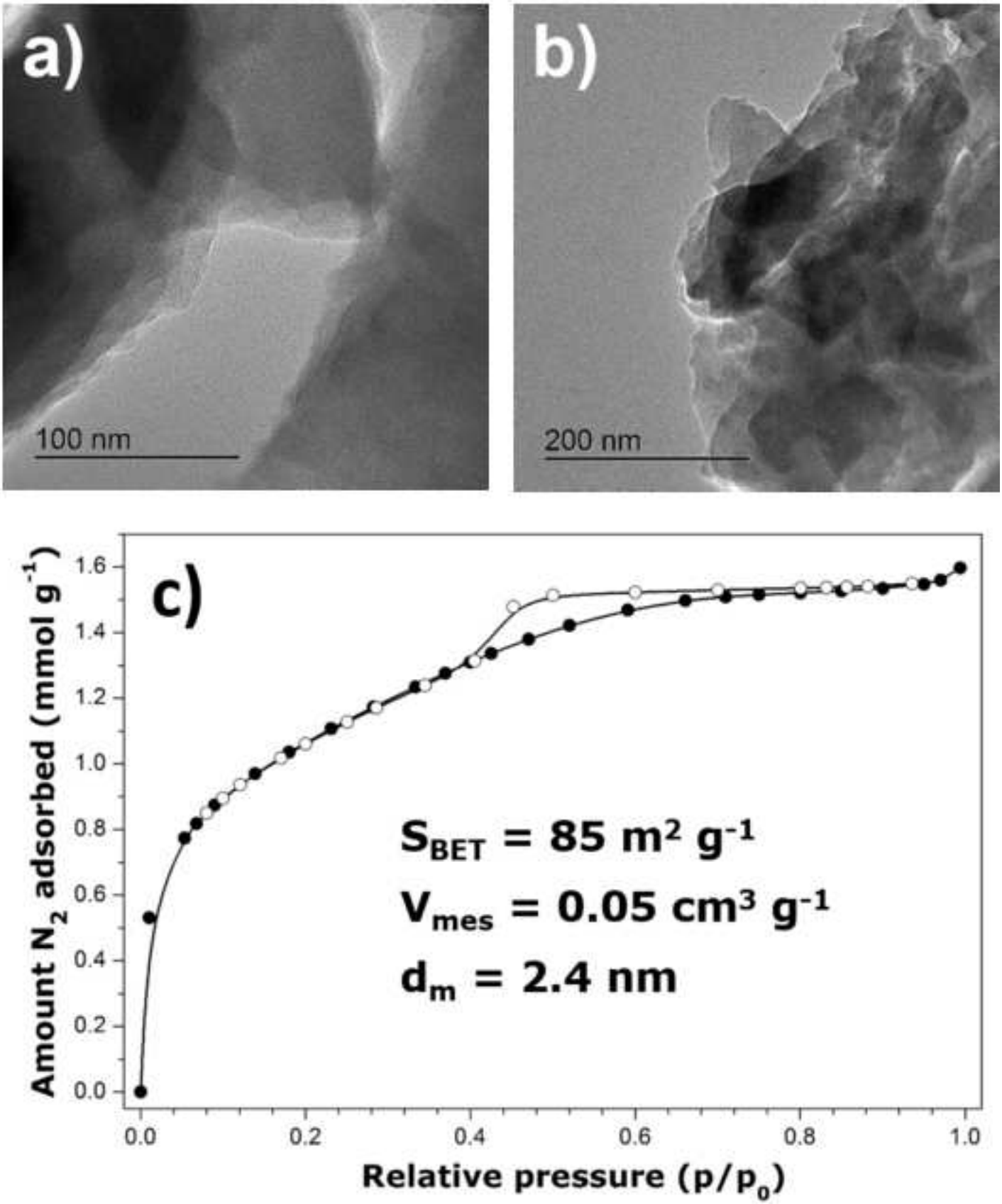

Figure 2

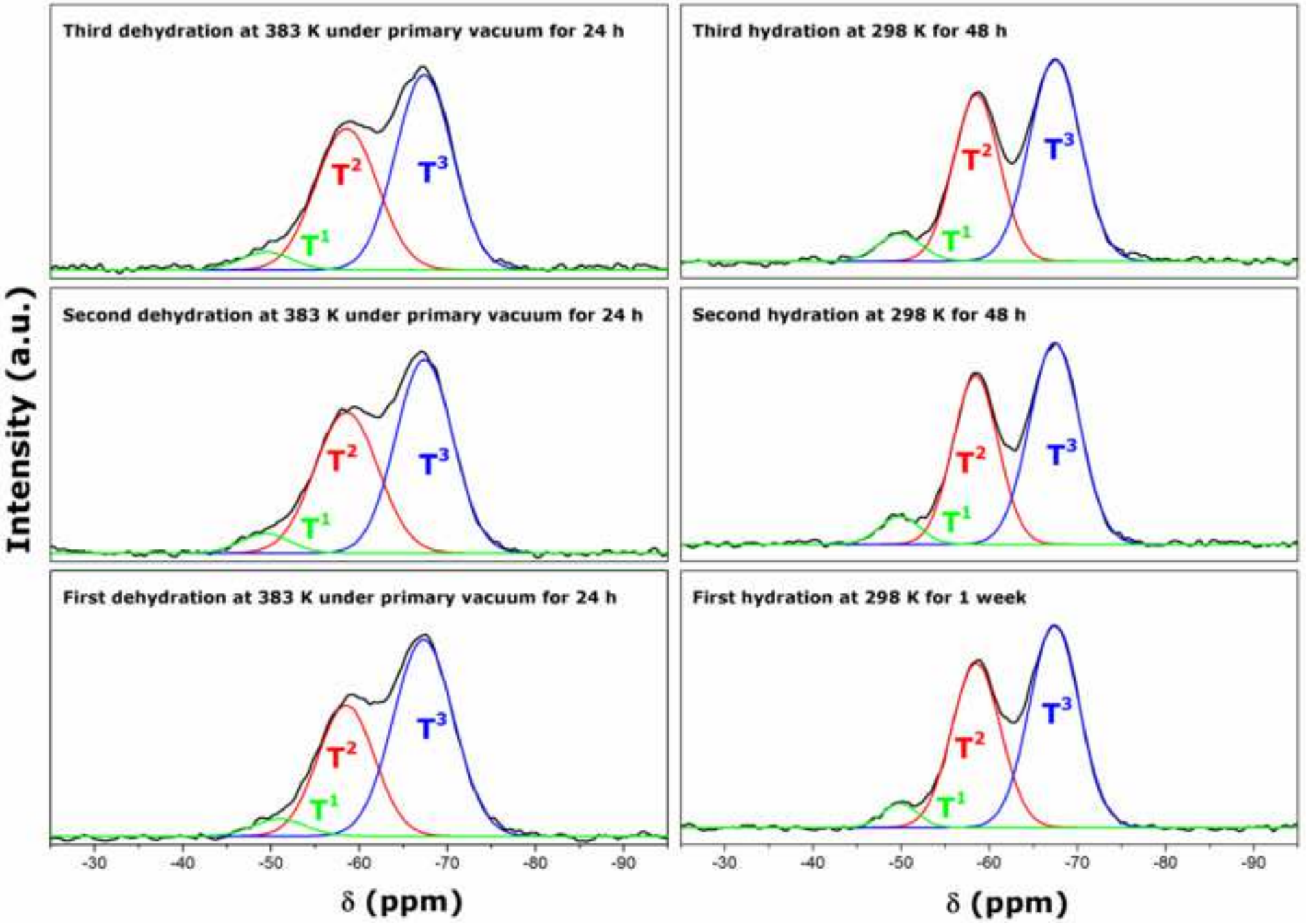

Figure 3

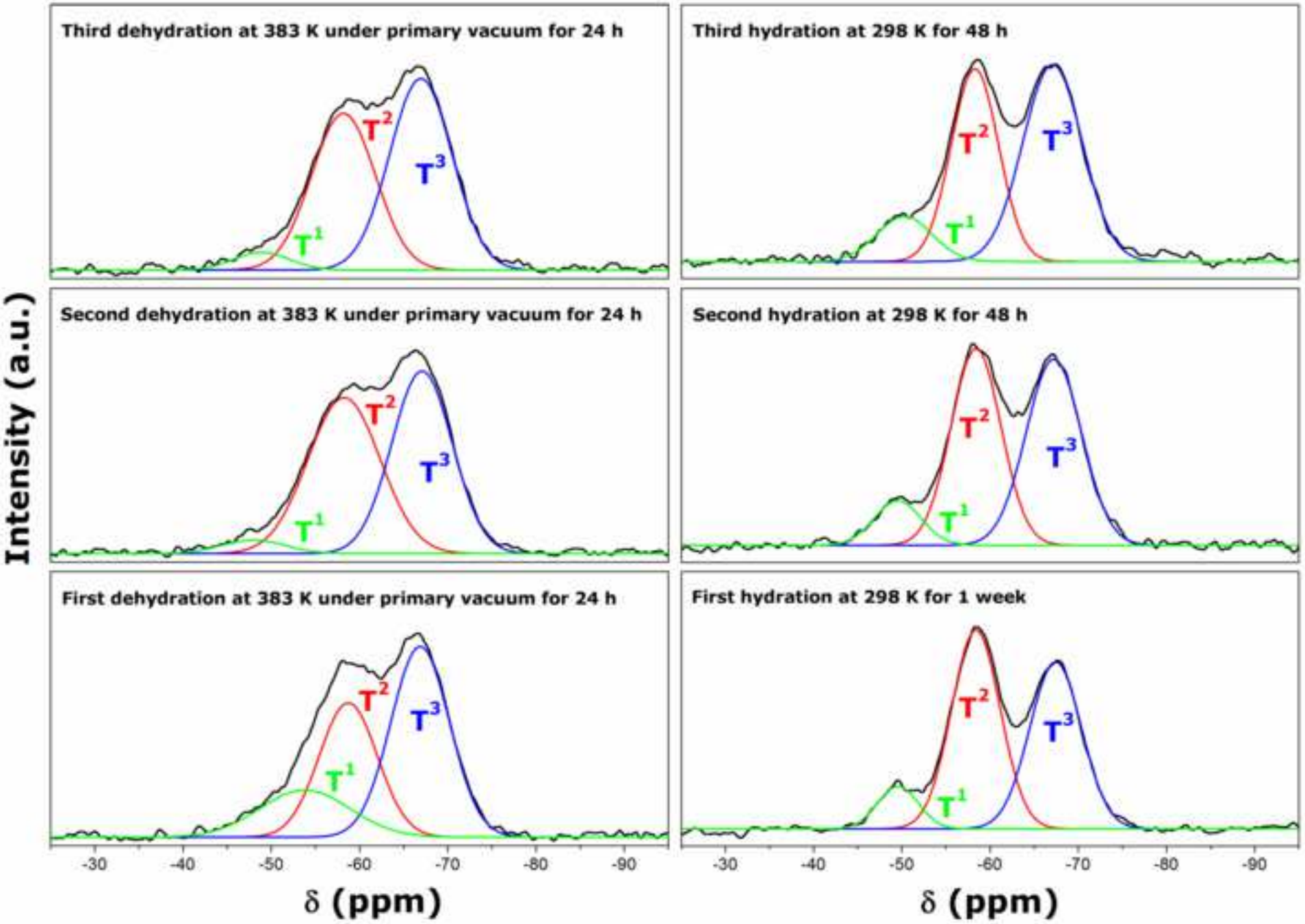

Figure 4

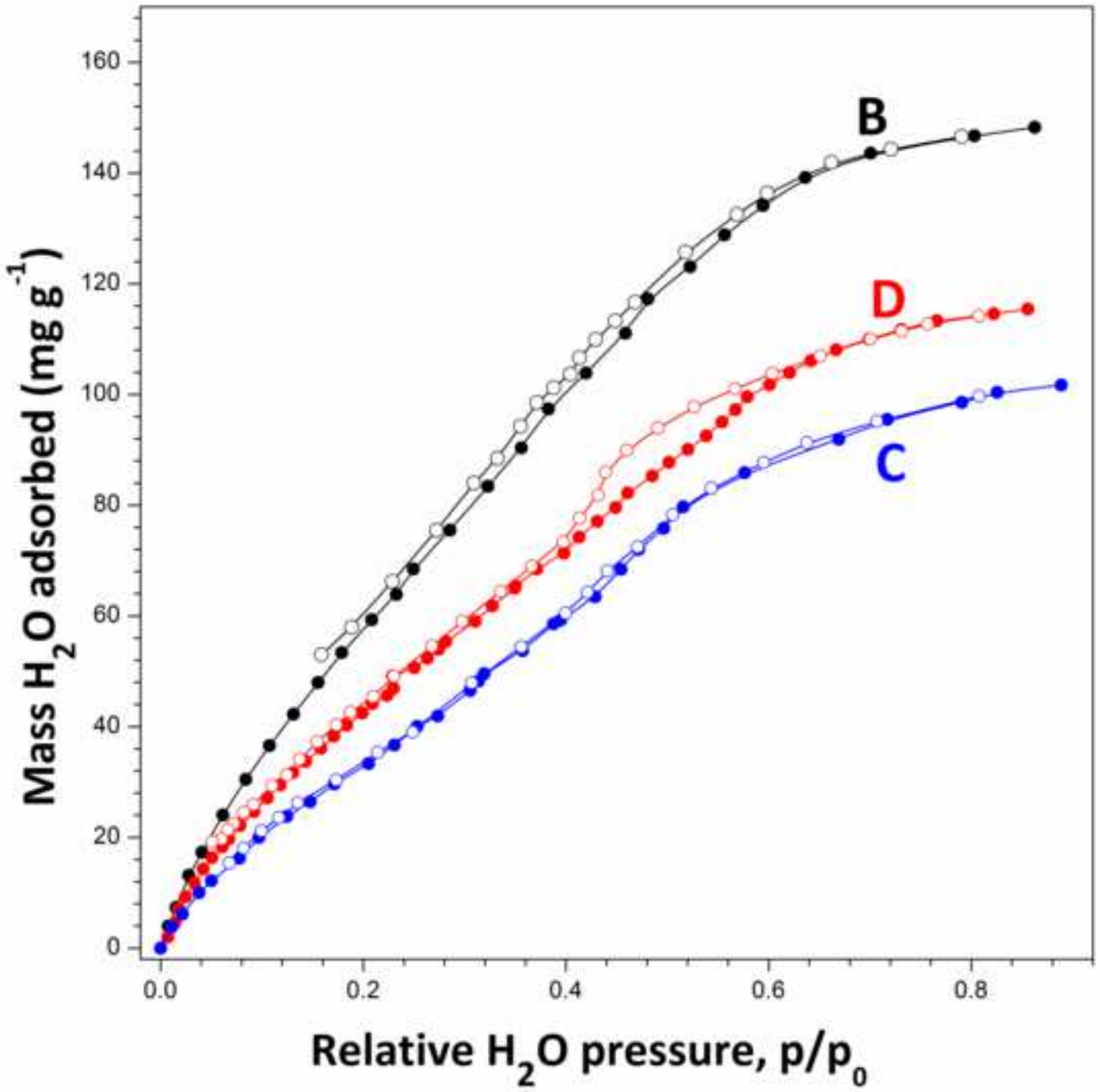

Figure 5

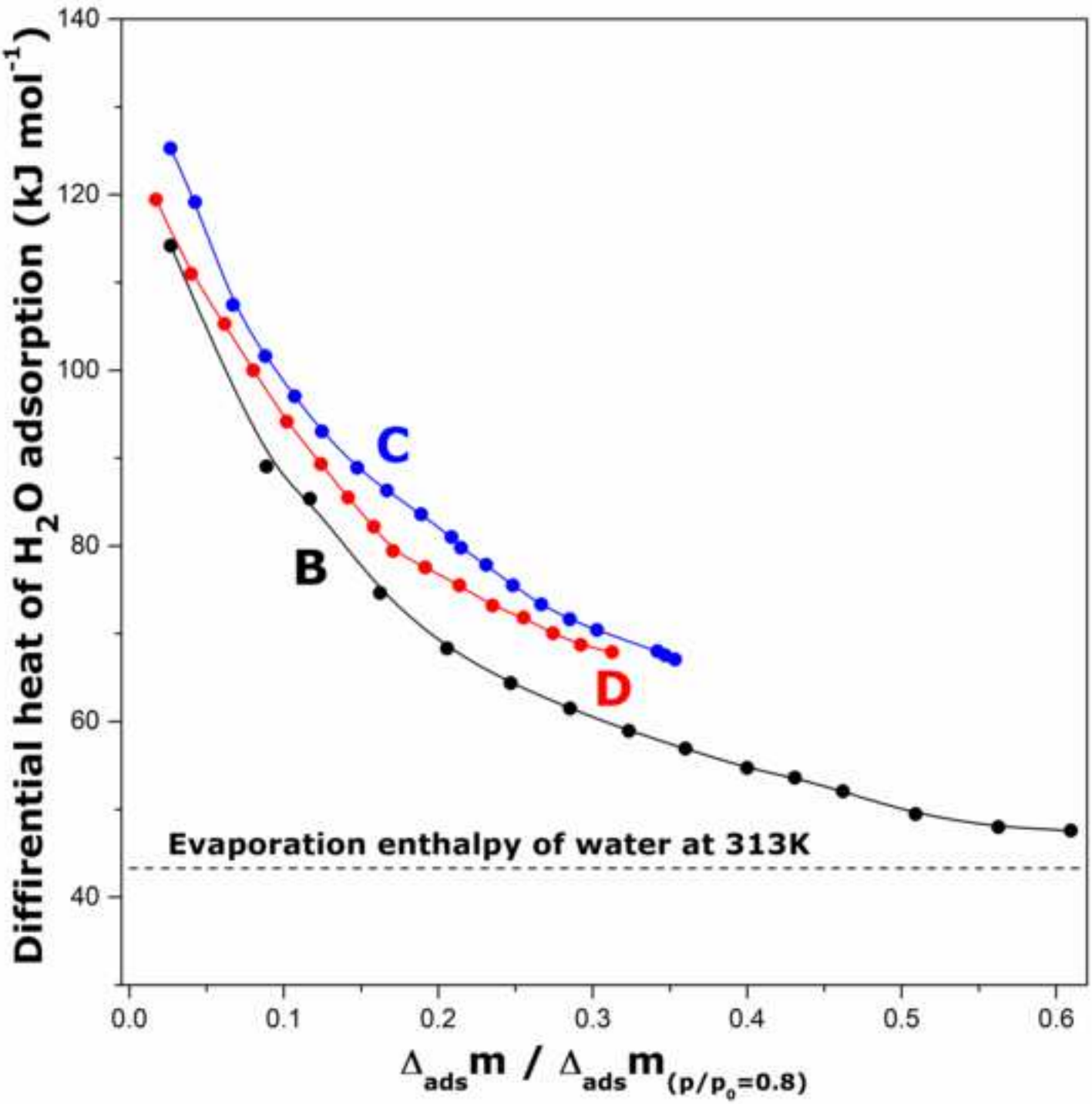

Figure 6

Click here to access/download;Figure;ZAJAC_Fig-6.tif